CellPress

Structure
Article

Inhibition Mechanism of Membrane Metalloprotease by an Exosite-Swiveling Conformational Antibody

Yael Udi,[1] Moran Grossman,[1] Inna Solomonov,[1] Orly Dym,[2] Haim Rozenberg,[2] Vanessa Moreno,[3] Philippe Cuniasse,[4] Vincent Dive,[4] Alicia García Arroyo,[3] and Irit Sagi[1,*]

[1]Department of Biological Regulation, The Weizmann Institute of Science, Rehovot 76100, Israel

[2]Structural Proteomics Unit and Department of Structural Biology, The Weizmann Institute of Science, Rehovot 76100, Israel

[3]Vascular Biology and Inflammation Department, Centro Nacional de Investigaciones Cardiovasculares (CNIC), Melchor Fernández Almagro 3, Madrid 28029, Spain

[4]Commissariat à l'Énergie Atomique et aux Énergies Alternatives (CEA), Service d'Ingénierie Moléculaire de Protéines, Gif/Yvette 91191, France

*Correspondence: irit.sagi@weizmann.ac.il

http://dx.doi.org/10.1016/j.str.2014.10.012

SUMMARY

Membrane type 1 metalloprotease (MT1-MMP) is a membrane-anchored, zinc-dependent protease. MT1-MMP is an important mediator of cell migration and invasion, and overexpression of this enzyme has been correlated with the malignancy of various tumor types. Therefore, modulators of MT1-MMP activity are proposed to possess therapeutic potential in numerous invasive diseases. Here we report the inhibition mode of MT1-MMP by LEM-2/15 antibody, which targets a surface epitope of MT1-MMP. Specifically, the crystal structures of Fab LEM-2/15 in complex with the MT1-MMP surface antigen suggest that conformational swiveling of the enzyme surface loop is required for effective binding and consequent inhibition of MT1-MMP activity on the cell membrane. This inhibition mechanism appears to be effective in controlling active MT1-MMP in endothelial cells and at the leading edge of migratory cancer cells.

INTRODUCTION

Proteases are a major class of enzymes involved in many physiological processes, such as extracellular matrix (ECM) remodeling, DNA replication and transcription, cell proliferation and differentiation, and angiogenesis (López-Otín and Matrisian, 2007a). Proteases were first considered as protein-degrading enzymes. However, over the years, it has been realized that they also play an important role as initiators of signaling cascades, in which proteases have distinct and specific roles in producing bioactive products (Liu et al., 2000; López-Otín and Overall, 2002; McQuibban et al., 2000; Wilson et al., 1999). Imbalanced protease activity is often associated with pathological states such as inflammation, cancer, and infectious diseases (López-Otín and Matrisian, 2007a; Turk, 2006a), making them highly important drug targets. For instance, overexpression of proteases belonging to structurally homologous families, such as cathepsin (Kawasaki et al., 2002; Koblinski et al., 2000), serine proteases (DeClerck and Imren, 1994), and matrix metalloproteinases (Choi et al., 2012), are associated with various clinical conditions.

MT1-MMP (membrane type I matrix metalloproteinase, MMP-14) belongs to a large family of zinc-dependent matrix metalloproteases (MMPs) consisting of more than 23 structurally homologous members as well as more than 50 related proteases (Bode et al., 1993). Beyond their key roles in ECM remodeling, the MMPs are also implicated in the proteolytic processing of other proteins, adhesion molecules, growth factors, cytokines, and hormones (Brinckerhoff and Matrisian, 2002). Consequently, these enzymes play key roles in many processes from cell proliferation, differentiation, and communication to pathological states associated with tumor metastasis, inflammation, tissue degeneration, and cell death (López-Otín and Matrisian, 2007a; Nagase and Woessner, 1999; Overall, 2002). MT1-MMP belongs to a subset of six membrane-tethered MMPs (MT1-MMP through MT6-MMP). MT1-MMP is involved in many cellular functions, including regulation of cell migration, invasion, angiogenesis, and induction of intracellular signaling pathways, and in the intracellular traffic of proteinases (Jiang et al., 2001; Lehti et al., 2000; Nakahara et al., 1997; Roghi et al., 2010; Rozanov et al., 2002; Seiki, 2003; Uekita et al., 2001; Wang et al., 2004). Its substrates include collagen types I, II, and III; gelatin; laminin; fibronectin; vitronectin; aggrecan; fibrin; and lumican (Itoh et al., 2006). In addition to ECM degradation, MT1-MMP also activates proMMP-2 and proMMP-13 by forming a complex of a homodimer of MT1-MMP together with a tissue inhibitor of metalloproteinase-2 (TIMP-2) molecule on the cell surface (Butler et al., 1998; Knäuper et al., 1996; Strongin et al., 1995). In addition, recent shotgun proteomics approaches have expanded the MT1-MMP substrate repertoire and identified a combinatorial proteolytic program driven by MT1-MMP during angiogenesis (Koziol et al., 2012a, 2012b).

MMPs, and MT1-MMP in particular, are well established targets for pharmaceutical development because of their tissue remodeling mechanisms and their regulatory roles in invasive diseases (Genís et al., 2006; Morrison et al., 2009). Most of the MMP inhibitors developed to date have been designed to target the active site zinc ion (Cuniasse et al., 2005; Fisher and Mobashery, 2006; Rao, 2005). However, these inhibitors displayed poor selectivity among the MMPs and other related enzymes because of the high structural homology at the active site (Overall and

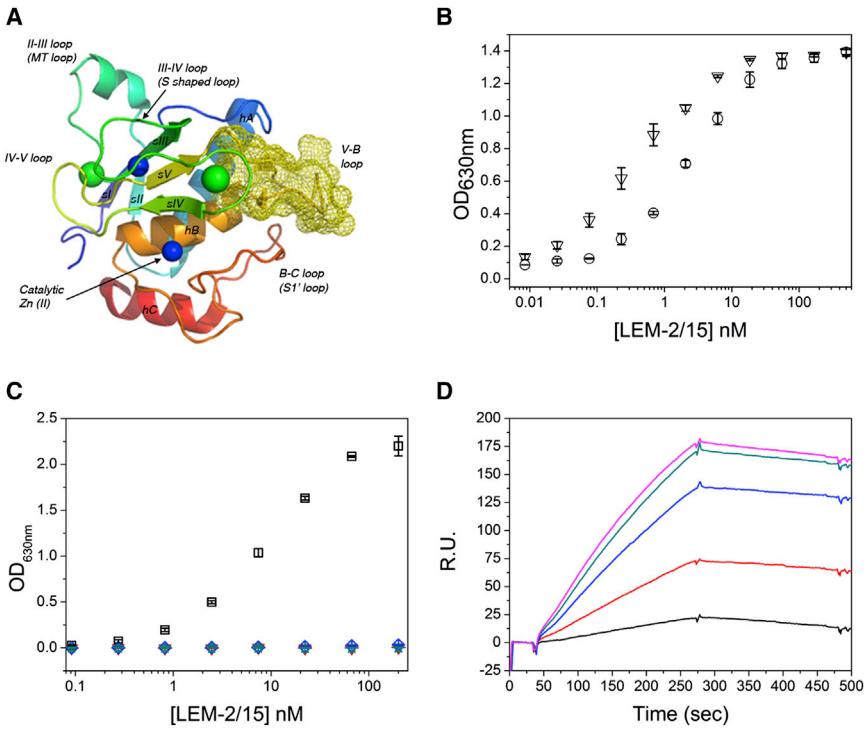

Figure 1. LEM-2/15 Binding to MT1-MMP

(A) CAT-MT1-MMP represented as ribbons. The catalytic and structural zinc ions are shown as blue spheres of arbitrary radii. The first and the second calcium ions are shown as green spheres. Strands and helices are labeled with numbers and Greek letters. The V-B loop is highlighted in yellow mesh.

(B) Binding curves for intact LEM-2/15 (▽) (K_D = 0.39 ± 0.05 nM) and the Fab (○) (K_D = 2.27 ± 0.12 nM) to CAT-MT1-MMP. Error bars represent SD of representative experiments done in triplicate.

(C) ELISA assay for LEM-2/15 binding to different catalytic domains of MMP family members: MT1-MMP (black), MMP-7 (red), MMP-9 (blue), and MMP-12 (green). Because the binding is highly selective toward MT1-MMP and the antibody does not bind the other MMPs tested, their symbols in the plot overlap. Error bars represent SD of representative experiments done in triplicate.

(D) SPR measurements of Fab LEM-2/15 binding to immobilized CAT-MT1-MMP: 2 nM (black), 5 nM (red), 10 nM (blue), 15 nM (green), and 20 nM (magenta) (ka^{app} = 2.76 × 10^5 M^{-1} s^{-1}, kd^{app} = 6.39 × 10^{-4} s^{-1} and K_D^{app} = 2.32 × 10^{-9} M).

López-Otín, 2002). Importantly, the failure of broad-range small-molecule inhibitors targeting the conserved MMP catalytic zinc sites revived the field's interest in designing specific inhibitors to control the pathophysiological activity of these enzymes in vivo (Deu et al., 2012; Sela-Passwell et al., 2010; Turk, 2006a). Therefore, targeting specific exosites residing outside of the conserved catalytic cleft has been suggested as an alternate drug design approach to control the destructive activity of MMPs in vivo (Sela-Passwell et al., 2010; Udi et al., 2013).

Monoclonal antibodies can serve as valuable reagents for specific targeting of exposed surface loops of proteases, and, therefore, can be tailored to target regulatory exosites. A set of three inhibitory antibodies targeted toward MT1-MMP, designated LEM (Gálvez et al., 2001a), was generated against two exposed loops of MT1-MMP (residues 160–173 and 218–233) by immunizing mice with these peptides. These antibodies inhibit the catalytic activity of MT1-MMP and further demonstrate antiangiogenic properties in cell-based assays (Gálvez et al., 2001a). However, the mechanism by which these antibodies control the enzymatic activity of MT1-MMP and how they achieve selectivity against other MMP family members is not clear. Therefore, understanding the mechanisms of their allosteric control is crucial to advance our knowledge regarding the selective and specific control of the enzymatic activity of MMPs for drug design.

Here we provide a detailed analysis of the interaction between MT1-MMP and the Fab fragment of the antibody LEM-2/15. This antibody was generated against the V-B loop of MT1-MMP situated above the specificity loop that connects β sheet V and α helix B (Figure 1A) and displays high sequence divergence among MMPs and, specifically, among the MT-MMP subfamily (Figures S1A and S1B available online). Kinetic and binding studies confirmed that this antibody and its Fab fragment are highly selective potent MT1-MMP inhibitors. The Fab fragment maintains the functional antibody properties in various biological assays, including in situ collagen zymography and proMMP-2 activation, together with the absent effect in MT1-MMP homodimerization. Using X-ray crystallography, we determined the structure of the free and bound Fab, suggesting conformational rearrangements of the enzyme scaffold to enable binding to the Fab fragment as a possible mechanism to control the enzymatic activity. Computational analyses further support our experimental observation, pointing to a role for conformational flexibility as mediating the function of this enzyme.

RESULTS

LEM-2/15 Is a Highly Selective Anti-MT1-MMP Antibody with Nanomolar Affinity

The antibody LEM-2/15 was generated by immunizing mice with a cyclic peptide possessing the sequence of the V-B loop, residues 218–233, which displays a unique sequence divergence within the MMP family members, as we have described previously (Gálvez et al., 2001a). To characterize the interaction between MT1-MMP and the antibody, we sequenced the antibody and generated a minimized antibody fragment, the Fab fragment, for easier handling and overexpression (Experimental Procedures and Supplemental Experimental Procedures). Noteworthy is that minimizing the size of the antibody may also offer an advantage in drug design. The Fab fragment was overexpressed in two ways: from the periplasmic space of *E. coli*, allowing simplified processing, enhanced biological activity, higher stability, and proper folding of the target protein (Mergulhão et al., 2005), and from the hybridoma clone culture supernatant of LEM-2/15 and by purification on a protein A column, followed

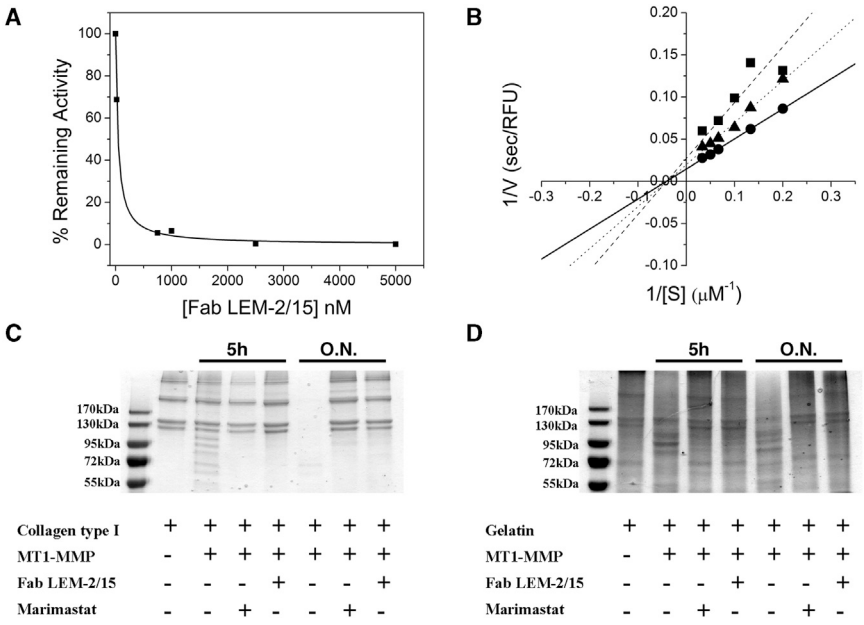

Figure 2. Inhibition of MT1-MMP Catalytic Activity by Fab LEM-2/15

(A) Dose-response curve for MT1-MMP inhibition by Fab LEM-2/15 using the 6-mer substrate (IC_{50} = 45 ± 2.4 nM).

(B) Lineweaver-Burk plots for MT1-MMP inhibition by Fab LEM-2/15 indicating noncompetitive inhibition. The Fab LEM-2/15 concentrations used were 0 nM (●), 250 nM (▲), and 500 nM (■).

(C) CAT-MT1-MMP (10 nM) was incubated with 1 mg/ml of collagen type I from rat tail in the absence or presence of 1 μM of Fab LEM-2/15 or 1 μM Marimastat, and samples were processed by 12% SDS-PAGE gel. Fab LEM-2/15 dramatically decreased the degradation process both after 5 hr (left lanes) and overnight (O.N., right lanes), similar to Marimastat.

(D) CAT-MT1-MMP (10 nM) was incubated with 10 mg/ml of gelatin in the absence or presence of 1 μM of Fab LEM-2/15 or 1 μM Marimastat, and samples were processed by 12% SDS-PAGE gel. Fab LEM-2/15 dramatically decreased the degradation process both after 5 hr (left lanes) and overnight (right lanes), similar to Marimastat.

by digestion with papain (Experimental Procedures) to produce the Fab fragment. To evaluate the potency of the generated Fab fragment toward MT1-MMP, we determined its binding affinity using ELISA assays and surface plasmon resonance (SPR). The affinity of the produced Fab fragments (recombinant and Fab from hybridoma) was tested against the catalytic domain of recombinant MT1-MMP (CAT-MT1-MMP) and compared with the binding of the intact antibody. Figure 1B shows the ELISA binding curves of both constructs, indicating that the intact antibody and the minimized Fab fragment possess comparable binding affinities at the nanomolar range, 0.4 and 2.3 nM, respectively. In addition, we further demonstrated that both the intact antibody and the Fab fragment recognize CAT-MT1-MMP and the catalytic hemopexin domain construct (CAT-HPX) of MT1-MMP with high affinity without any steric hindrance of the hemopexin domain to LEM-2/15 (Figures S2A and S2B). Because the catalytic domain of the MMP members share high structural homology, we further investigated the selectivity of the Fab fragment toward MT1-MMP over other MMP members, including MMP-7, MMP-9, and MMP-12, using an ELISA assay as well as an ELISA competition assay. Remarkably, in both experiments, the Fab fragment was highly selective toward MT1-MMP over the other MMPs tested (Figure 1C; Figure S2C). This result is consistent with the sequence divergence of the V-B loop among the MMPs used to immunize the mice to generate the LEM-2/15 antibody.

To obtain information regarding the binding kinetics of the MT1-MMP:Fab complex, we performed a real-time SPR analysis. Diluted solutions of Fab LEM-2/15 were injected over surface-immobilized CAT-MT1-MMP as we monitored the progress of the binding over time. The changes in the SPR resonance, due to changes in mass as a result of binding, were measured (Figure 1D). The SPR analysis revealed that the Fab fragment binds CAT-MT1-MMP with a kinetic association (ka^{app}) of 2.76 × 10^5 M^{-1} s^{-1}, a kinetic dissociation (kd^{app}) of 6.39 × 10^{-4} s^{-1}, and a dissociation constant (K_D^{app}) of 2.32 × 10^{-9} M. In addition, the formation of the Fab:enzyme complex was observed by size exclusion chromatography (Figure S3A). The eluted complex was identified according to its elution volume to have a molecular weight of ~70 kDa, and its content was confirmed by 12% SDS-PAGE gel (Figure S3B) to be composed of the CAT-MT1-MMP and the Fab LEM-2/15. This experiment further indicates the formation of a high-affinity complex in solution.

Fab LEM-2/15 Inhibits the Catalytic Activity of MT1-MMP In Vitro

The effect of the Fab fragment on the enzymatic activity of CAT-MT1-MMP was tested using three substrates. We first performed enzyme kinetic assays on a small, fluorogenic, six-amino acid substrate according to a standard procedure (Knight et al., 1992). The enzymatic activity of recombinant CAT-MT1-MMP was measured in the presence of increasing concentrations of Fab LEM-2/15. Figure 2A shows the dose-response curve for CAT-MT1-MMP inhibition with a half-maximal inhibitory concentration (IC_{50}) value of 45 ± 2.4 nM, demonstrating the high potency of this Fab fragment as an inhibitor of the enzymatic activity. Further kinetic analyses were performed to determine the type of inhibition achieved by the Fab fragment. For this purpose, a series of enzymatic activity assays using different Fab fragment concentrations were performed. The obtained Lineweaver-Burk plots (Figure 2B) demonstrate that the inhibition profile shows a noncompetitive inhibition pattern. This was also indicated by the kinetic parameters derived from the Lineweaver-Burk plots (Table 1), where the maximum velocity (V_{max}) is reduced with the increase of LEM-2/15 concentration, whereas the affinity to the substrate (K_M) remained unchanged. Therefore, Fab LEM-2/15 does not compete with the binding of the small substrate at the catalytic zinc ion. This result indicates that the Fab LEM-2/15 modulates the catalytic activity by binding at the

Table 1. The Kinetic Activity of MT1-MMP in the Presence of LEM-2/15

[LEM-2/15] nM	V_{max} (RFU/s)	K_M (uM)
0	68.3	24.3
250	50.5	25.1
500	36.9	24.4

V-B loop located away from the active site and not by sterically hindering it. We further evaluated the effect of the Fab fragment on the enzymatic degradation of two physiological substrates of MT1-MMP, collagen type I and gelatin. CAT-MT1-MMP was incubated in the presence of Fab LEM-2/15 and added to samples of collagen type I or gelatin. Marimastat, a broad-spectrum inhibitor of MMPs that binds to the zinc ion, was used as a positive control to compare the degradation pattern with a known potent inhibitor (Coussens et al., 2002; Rasmussen and McCann, 1997). The samples were analyzed by 12% SDS-PAGE gel after 5 and 16 hr, both analyses showing that the inhibitors prevented the degradation of the substrates into low-molecular-weight products (Figures 2C and 2D). Importantly, the inhibitory effect of Fab LEM-2/15 on naturally occurring substrates reveals a pronounced effect, demonstrating its inhibitory potency on physiological substrates.

Structural Comparison of the Free Fab and the MT1-MMP:Fab Complex

To determine how LEM-2/15 inhibits the catalytic activity of CAT-MT1-MMP, we characterized their interaction by protein crystallography. We obtained crystal structures of the free Fab fragment at 2.6 Å resolution, two crystal forms of the Fab fragment in complex with a segment of the V-B loop (residues 215–227) that diffracted to 1.94 and 1.95 Å, and another crystal structure of the Fab fragment in complex with a segment of the V-B loop (residues 218–228) (Figure 3A; Figure S4A). (Data collection and crystallographic refinement statistics are available in Table S1.) All three structures of the Fab fragment coincide with the structure of the free Fab with a root-mean-square deviation (rmsd) of 0.4 Å (Figure S4A). Moreover, the V-B loop observed in the structures align with an rmsd of 0.05 Å for the structures with the 215–227 segment and an rmsd of 0.5 Å for the 215–227 and 218–228 segments. Figures S4B and S4C show their structural alignment. The Fab fragment structure exhibits a typical architecture of antibodies, with a binding site lined by residues of the complementarity-determining regions (CDRs). The CDRs are assigned to known canonical structure classes according to Chothia et al. (1989) (Table 2). However, they form a relatively narrow antigen binding site compared with other antibodies targeted against macromolecules (Wilson and Stanfield, 1994). The crystal structures of the complex reveal that the bound peptide interacts with all six CDRs through various types of interactions (Figures 3B and 3C; Table 3). The major interactions occur within residues Trp221 through Arg224. The side chain of Trp221 forms a hydrogen bond and π-π interactions with the side chain of Tyr101 (CDR L3) in addition to π-π interactions with the side chain of Phe105 (H3). The side chain of Thr222 forms hydrogen bonds with Gly53 (H2). In addition, the side chain of Arg224 forms a salt bridge with Glu39 (L1) and a cation-π interaction with Tyr101 (L3) (Figure 3C). These highly energetic interactions rationalize the high-affinity interaction between CAT-MT1-MMP and the Fab fragment, and it points the loop toward the conformation observed in the crystal structure. Interestingly, the conformation of the C-terminal part of the bound peptide deviates from its corresponding segment in the crystal structure of CAT-MT1-MMP in complex with TIMP-1 (Grossman et al., 2010) and TIMP-2 (Fernandez-Catalan et al., 1998) because of the interaction of the Trp221 side chain with the Fab fragment binding pocket (Figures 3A–3C). Importantly, the side chains of both Trp221 and Arg224, when MT1-MMP is bound to TIMP, point toward the core of the enzyme, whereas, in our structure, they point outside, toward the binding site of the Fab fragment. Therefore, it is reasonable to assume that the binding to the Fab fragment induces these conformational changes. In addition, the Fab residues that interact with Trp221 and Arg224 of the MT1-MMP in the structure adopt a similar orientation in the free Fab structure (Figure S4A), which further supports the assumption that the change in the orientation of Trp221 and Arg224 of the MT1-MMP is induced by binding to the Fab. The comparison between the bound fragment and its corresponding epitope from the MT1-MMP:TIMP structure is shown in Figures 4B and 4C and Table S2. The major changes of the torsional angles clearly demonstrate that there is a change in conformation of the C-terminal part of the bound MT1-MMP fragment affecting both Cα and the side chains. Another significant change observed in the structure is the distance between the Cα of Trp221 and Arg224. In our structure, the calculated distance is 5.6 Å, whereas, in the structure of MT1-MMP in complex with TIMP-1, the distance is as twice as long, 10.7 Å (Figures 4B and 4C). This effect may arise because of the conformational restriction imposed by immunizing with a cyclic peptide corresponding to the sequence of residues 218–233 of MT1-MMP (Gálvez et al., 2001a). Therefore, this immunization strategy resulted in an inhibitory antibody that induces the conformational change according to its target conformation. Taking these findings together, we propose that the conformational swiveling motion of the V-B loop is critical in mediating the interaction between the Fab fragment and the enzyme. The obtained crystal structures demonstrate that binding of MT1-MMP to the inhibitory Fab fragment is mediated by highly energetic interactions and involves the conformational rearrangement of the enzyme scaffold controlling the enzymatic activity.

To test the possibility of the swiveling mechanism and, specifically, the existence of the observed V-B loop conformation within the ensemble of the possible conformations accessible to this loop in the context of the CAT- MT1-MMP in solution, we performed targeted molecular dynamics (TMD) simulations. The simulation started from the conformation of CAT-MT1-MMP as observed in its TIMP-1 complex (Protein Data Bank [PDB] ID code 3MA2; Grossman et al., 2010). The targeted conformation of CAT-MT1-MMP was defined using the coordinates of 3MA2 for all residues of the catalytic domain, with the exception of residues 215–228, whose coordinates were taken from that observed for the peptide in complex with the LEM-2/15 Fab. The rmsd of the 215–228 atoms between the starting and the targeted conformation was about 3.0 Å. During the TMD simulation this RMSD was gradually reduced to about 0.5Å (Figure S5). The final TMD structure of free

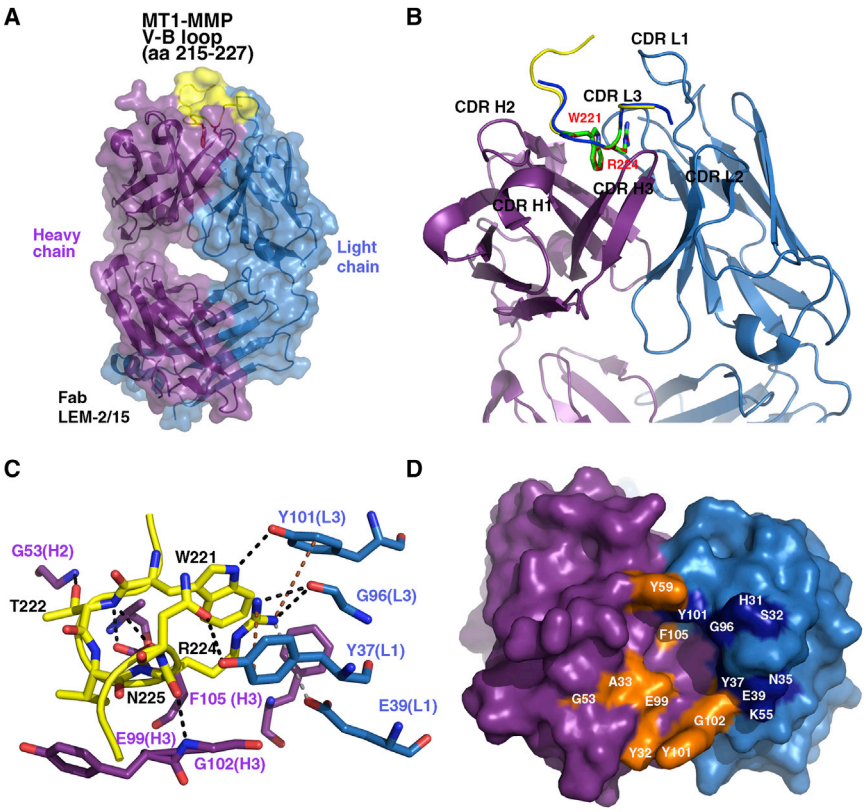

Figure 3. Structural Analyses of the Fab Fragment with Its Antigen

(A) Surface representation with the secondary structure highlighted for the complex between the V-B loop of MT1-MMP (yellow) and Fab LEM-2/15 (light chain in blue, heavy chain in purple).

(B) Secondary structure representation of a close view of interactions of CDR loops of Fab LEM-2/15 with the V-B loop. Central residues involved in the binding interactions are highlighted in red (Trp221 and Arg224).

(C) Stick representation of the CDR residues interacting with the V-B loop fragment of MT1-MMP. Shown are hydrogen bond (black dashed line), cation-π (brown dashed line), and electrostatic interactions (light gray dashed line) between Trp221 and Asn225 (yellow) and the Fab CDRs (light chain in blue, heavy chain in purple).

(D) The V-B loop contact region on Fab LEM-2/15 (heavy chain contacts in orange, light chain contacts in dark blue).

CAT-MT1-MMP (after a final step of energy minimization) shown in Figures 4A and 4D shows an excellent agreement of the peptide 218–227 conformation with that observed in the Fab complex. During the conformational transition between the starting structure and the targeted one, no dramatic increase in total energy of the system or unrealistic conformational distortion of the catalytic domain were observed. This suggests a possible low-energy barrier between the two conformations (Figure S5). The absence of a significant increase in total energy of the system in conjunction with the preservation of the structure of CAT-MT1-MMP during the transition driven by the artificial potential V_{rmsd} argue for a possible population of this conformation of the 215–227 peptide in the CAT-MT1-MMP in water solution. To further estimate the stability of the final TMD conformation obtained under rmsd restraints, we carried out a 10 ns unrestrained molecular dynamics (MD) simulation in water solution. We monitored the rmsd on the positions of the Cα atoms along this trajectory compared with the final TMD conformation of CAT-MT1-MMP. Two sets of atoms were considered. Set 1 corresponded to Cα atoms of residues 215–228, and set 2 corresponded to all Cα atoms of the CAT-MT1-MMP, with the exception of the 215–233 region. The atoms of set 2 were used to superimpose the structures of CAT-MT1-MMP of the different frames analyzed by minimizing the rmsd on the position of their coordinates with that of the starting MD structure (the final TMD one). In this unrestrained MD simulation, the rmsds on the coordinates of set 1 rapidly reached a value of about 5.0 Å compared with the starting structure, whereas the rmsd corresponding to set 2 remained below 2.0 Å (Figure S6). This observation strongly suggests that the targeted TMD conformation of region 215–228 is not stable along the unrestrained MD trajectory in the context of the CAT-MT1-MMP at the free state. A similar conclusion can be drawn from the analysis of the ϕ and ψ dihedral angles and the values of certain ϕ-ψ angles obtained (data not shown). Therefore, this conformation is likely energetically less favorable in the free enzyme and possibly only stabilized by the interaction with the LEM-2/15. This mode of inhibition affects the enzymatic activity of MT1-MMP in vitro by targeting hidden regulatory exosites together with affecting the conformational population in solution, which results in allosteric control of the enzymatic function.

The conformational rearrangement suggested by the crystal structure was confirmed by 1-anilinonaphthalene-8-sulfonic acid (ANS) fluorescence assay. Typically, the fluorescence of ANS is low in water solution and increases upon hydrophobic interactions. This phenomenon makes ANS a sensitive probe to detect conformational changes involving exposure of hydrophobic patches (Arighi et al., 1998; Raha et al., 1999). ANS emission spectra (400–600 nm) were recorded in the presence of 5 μM CAT-MT1-MMP, 5 μM Fab LEM-2/15, or the complex MT1-MMP:Fab LEM-2/15. In the presence of each of the proteins, ANS fluorescence did not change significantly, suggesting only little binding of the probe to each of the proteins separately. However, in the presence of the complex, ANS fluorescence increased significantly (Figure 5A), indicating the exposure of a hydrophobic surface area formed as a result of the conformational rearrangement induced by binding of Fab LEM-2/15. To reveal the structural basis for the observed conformational change, we compared the MT1-MMP TMD structure (containing the swiveled V-B loop) with the known MT1-MMP crystal structure (PDB ID code 3MA2, in which the V-B loop adopts its non-swiveled conformation). Remarkably, we observed a larger hydrophobic surface area in the TMD structure, resulting, upon swiveling of the V-B loop, in the calculated MT1-MMP structural model corresponding to the binding of Fab LEM-2/15 (Figures

Table 2. Canonical Classes of Hypervariable Loops of Fab LEM-2/15

CDR	Residue Numbering	Canonical Class[a]	PDB ID Code
L1	24–39	4	1RMF
L2	55–61	1	1LMK
L3	94–102	1	1TET
H1	26–35	1	2FBJ
H2	50–58	3	1IGC
H3	99–107	–	–

[a]Structural classification according to http://www.bioinf.org.uk/abs/chothia.html.

Table 3. Interactions Formed between the V-B Loop Residues and the Fab Fragment

V-B Loop Residue Number[a]	Fab Fragment Residue Number	Type of Interaction	CDR
Phe215	Ser32	H bond	L1
Asp216	Tyr59	H bond	H2
Ser217	–	–	–
Ala218	–	–	–
Glu219	His31	H bond	L1
Pro220	Tyr59	hydrophobic	H2
Trp221	Ala33	hydrophobic	H1
	Phe105	hydrophobic, π-π	H3
	Tyr101	hydrophobic, H bond, π-π	L3
Thr222	Gly53	H bond	H2
	Glu99	H bond	H3
Val223	Tyr32	hydrophobic	H1
	Tyr101	hydrophobic	H3
Arg224	Gly102	H bond	H3
	Glu99	H bond	H3
	Gly96	H bond	L3
	Tyr37	cation-π	L1
	Tyr101	cation-π	L3
	Glu39	Ionic	L1
Asn225	Tyr37	H bond	L1
Glu226	–	–	–
Asp227	Asn35	H bond	L1
	Lys55	H bond, ionic	L2

[a]The underlined residues are the residues forming the major interactions with the CDRs.

5C and 5D). The side chains of Trp221 and Trp263 point outward and contribute to a larger hydrophobic surface area, and a new hydrophobic patch is formed by the side chains of Val223 and Leu228. Accordingly, a significant change in the electrostatic surface potential also occurs (Figures 5E and 5F), resulting in partial loss of the negative electrostatic potential of the V-B loop and formation of a negatively charged region in the cavity formed by the V-B loop and α helix A. All of these changes may affect the interaction of MT1-MMP with its physiological substrates in vivo, which may require additional protein-protein interaction on the surface of MT1-MMP. Aside from the changes in hydrophobicity and electrostatic potential, Figures 5D and 5F clearly demonstrate that the catalytic cleft adopts a narrower conformation upon swiveling of the V-B loop. Finally, to identify changes at the zinc active site, we performed X-ray absorption spectroscopy (XAS). XAS evaluates the ligand environment of the nearest coordination shell of the protein-bound metal ion and, additionally, the metal electronic structure (up to 4 Å). This technique is ideal for obtaining accurate and precise solution structural data of metal ion complexes within the active sites of metalloproteins (Frenkel et al., 2002; Sharma, 2012). The XAS data of CAT-MT1-MMP in complex with Fab LEM-2/15 were collected and analyzed (Figure 5B; Table S3). No changes in spectral features or in the structural parameters of the catalytic zinc histidine-nearest environment were detected upon binding of Fab LEM-2/15 to CAT-MT1-MMP (Table S3; Grossman et al., 2011; Udi et al., 2013). These results further indicate that the structural changes of MT1-MMP occur at exosite regions, and, therefore, it further supports the observed noncompetitive mode of inhibition by Fab LEM-2/15.

Fab LEM-2/15 Affects the Catalytic Activity of MT1-MMP in Cells, but It Does Not Impair Noncatalytic Functions

To demonstrate the effect of the allosteric inhibition on cellular activities of MT1-MMP, we performed functional assays where MT1-MMP is known to play a key role in collagen degradation, proMMP-2 activation, and homodimerization. Localization of collagenolytic activity in cells is possible with the addition a fluorescently quenched collagen type I (DQ-collagen). After cleavage by MT1-MMP, fluorescent peptides are produced and can by visualized and quantified (Bahar et al., 2007; Kay et al., 1992). This functional assay was done using a human fibrosarcoma cell line (HT1080) that overexpress MT1-MMP, and the localization of collagenolytic activity was detected as green fluorescent areas because of DQ-collagen degradation. Cells treated with Fab LEM-2/15 displayed reduced collagen fluorescence, indicating a dose-dependent reduction in collagenolytic activity (Figures 6A and 6B), leading to a 75% decrease in localized fluorescence in the presence of 5 μM Fab LEM-2/15. Therefore, although LEM-2/15 does not bind at the active site, it impairs the collagenase activity of the intact enzyme in the native extracellular environment against a natural substrate.

The role of MT1-MMP is not restricted to degradation of the ECM components, and it was the first member of the MMP family identified as physiologic activator of proMMP-2 (Browner et al., 1995). This activation process is thought to be critical in cancer invasion (Sato et al., 1994) and growth (Taniwaki et al., 2007) because activated MMP-2 can degrade collagen type IV whereas MT1-MMP does not. To test the effect of Fab LEM-2/15 on the activation of proMMP-2 by MT1-MMP (Koshland and Hamadani, 2002; Monod et al., 1965), human endothelial cells were stimulated by wounding and the chemokine MCP-1 to initiate the activation process in the presence of increasing concentrations of Fab LEM-2/15 or control immunoglobulin G (IgG). Figure 6C demonstrates a moderate inhibitory effect of Fab LEM-2/15 on proMMP-2 activation.

Finally, we tested the effect of Fab LEM-2/15 on the noncatalytic activity of MT1-MMP. MT1-MMP forms homodimers on the

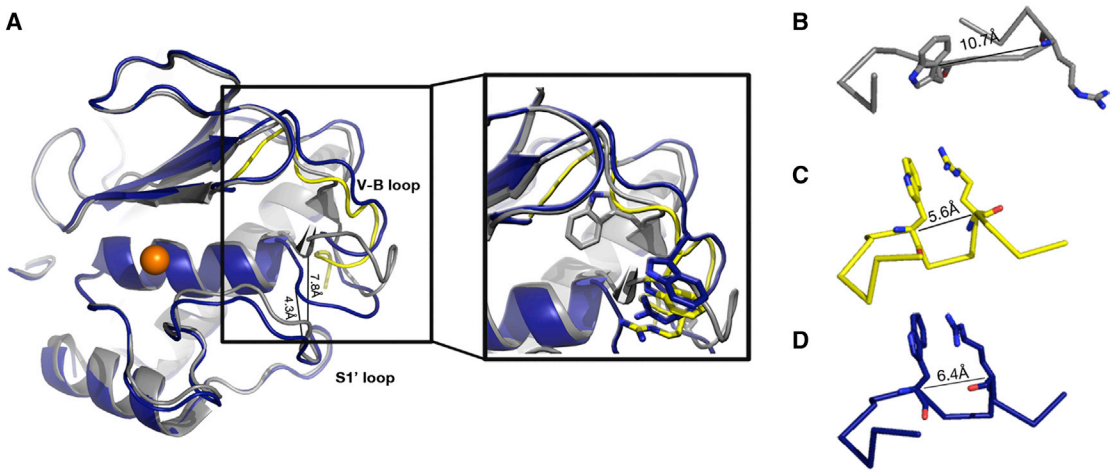

Figure 4. TMD Demonstrating the Possibility of the V-B Loop to Accommodate the Conformation Observed in the Crystal Structure

(A) Superposition of the secondary structure representation of the TMD structure (blue) with the MT1-MMP structure (gray) (Grossman et al., 2010; PDB ID code 3MA2) and the V-B loop in our structure (yellow). The inset shows a close-up view of the V-B loop region.

(B) Ribbon representation of residues 216–227 and the distance between the Cα of Trp221 and Arg224 from PDB ID code 3MA2 (Grossman et al., 2010).

(C) Ribbon representation of residues 216–227 and the distance between the Cα of Trp221 and Arg224 from PDB ID code 4P3D.

(D) Ribbon representation of residues 216–227 and the distance between the Cα of Trp221 and Arg224 from the TMD structure.

cell surface. This dimerization process was found to be crucial for proMMP-2 activation and cleavage of collagen type I fibers at the cell surface (Itoh et al., 2006). No significant effect on homodimerization was detected in the presence of increasing concentrations of Fab LEM-2/15 or control IgG in activated human endothelial cells (Figure 6D). Therefore, the Fab fragment interacts specifically with the MT1-MMP expressed on the cell surface and inhibits mostly its collagenase activity while not interfering significantly with the activation of proMMP-2 and the enzyme dimerization on the cell surface. This highly selective inhibitory profile of LEM-2/15 may be relevant to other pathologies, such as infection, inflammation, and specific cancer processes, in which activation of proMMP-2 is beneficial whereas the collagenase activity by MT1-MMP is destructive. Overall, we directly demonstrate that the Fab fragment controls the enzymatic activity of MT1-MMP on various substrates both in vitro and in live cells.

DISCUSSION

In this work, we obtained and characterized a highly specific and potent Fab fragment inhibitor of MT1-MMP. This Fab fragment is selective toward MT1-MMP over other highly homologous family members, and it inhibits the enzymatic activity in a noncompetitive manner, suggesting an allosteric mechanism of inhibition. LEM-2/15 forms a high-affinity complex with MT1-MMP (in the nanomolar range), and it inhibits the proteolytic activity of MT1-MMP against a range of substrates. Structural comparison between the free Fab fragment and in complex with a small segment of MT1-MMP suggests that the enzyme undergoes major conformational changes during binding to LEM-2/15. Specifically, for the LEM-2/15 to bind Trp221 of MT1-MMP, the V-B loop of the later has to "flip out" toward the antibody. This change at the V-B loop leads to narrowing of the substrate binding cleft as the distance between the V-B loop and the S1′ specificity loop is shortened from 7.8 Å between the Cα of Asn231and the Cα of Trp263 in the structure of MT1-MMP:TIMP-1 (Grossman et al., 2010) to 4.3 Å in our TMD structure (Figure 4A). It has been established that the V-B loop plays a role in the collagenolytic activity for MMP-1 (Chung et al., 2000), MMP-8 (Pelman et al., 2005), and MMP-12 (Bhaskaran et al., 2008; Chung et al., 2000; Palmier et al., 2010) because it serves as a binding site for collagen. Although such a role has not yet been investigated for MT1-MMP, it is reasonable that the V-B loop serves a similar role. In addition, in a previous study, we demonstrated that this loop serves as a potential hidden regulatory site on MT1-MMP, and nuclear magnetic resonance (NMR) analyses have also demonstrated that this loop is highly flexible (Udi et al., 2013). Based on the results discussed above, we would like to offer three possible mechanisms for the inhibition: (1) Narrowing the substrate binding cleft between the V-B loop and the S1′ may prevent substrate binding. (2) Constraining the flexibility of the loop upon binding may alter the intrinsic dynamics of the enzyme necessary for proper activity and substrate binding. (3) A combination of (1) and (2), where the combination of constrained dynamics and conformational rearrangement of the V-B loop during binding of the antibody constitute the basis of the allosteric nature of the antibody.

Our results demonstrate that LEM-2/15 inhibits mostly the collagenase activity of MT1-MMP while not interfering significantly with the activation of proMMP-2 and not affecting the enzyme dimerization on the cell surface. Importantly, there are specific stages in cancer progression in which activation of proMMP-2 is beneficial, whereas uncontrolled MT1-MMP-mediated collagen degradation is destructive (Genís et al., 2006; McQuibban et al., 2000; Overall and Kleifeld, 2006). Therefore, inhibiting only the collagenolytic activity, while not affecting other important biological processes mediated by MT1-MMP, may be superior over inhibitors blocking proMMP-2 activation in various pathologies such as inflammation and infection diseases as well

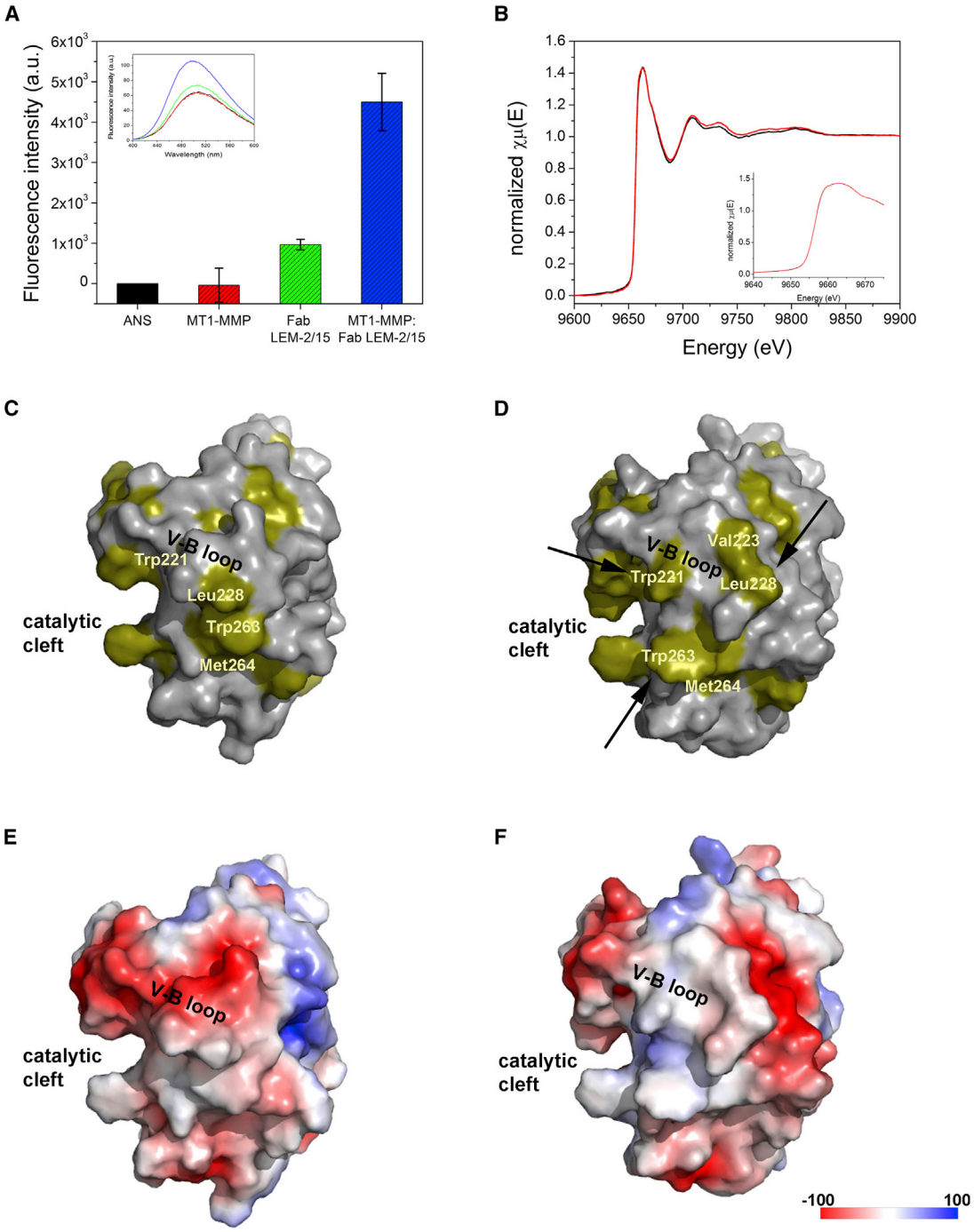

Figure 5. Changes in the Surface Properties of MT1-MMP Induced by LEM-2/15 Binding

(A) ANS fluorescence assay. ANS (250 μM) was added to CAT-MT1-MMP (5 μM), Fab LEM-2/15 (5 μM), and a 1:1 complex. The samples were excited at 350 nm, and fluorescence spectra (400–600 nm) were recorded. The fluorescence intensity was calculated as the area of the spectra at 400–600 nm (ANS, black; MT1-MMP, red; Fab LEM-2/15, green; MT1-MMP:Fab LEM-2/15, blue). The inset shows emission spectra of the proteins in the presence of ANS (ANS, black; MT1-MMP, red; Fab LEM-2/15, green; MT1-MMP:Fab LEM-2/15, blue). Error bars represent SD of representative experiments done in triplicate. a.u., arbitrary units.

(B) X-ray absorption spectra. Binding of Fab LEM-2/15 to CAT-MT1-MMP did not alter the zinc ion environment (CAT-MT1-MMP, black; CAT-MT1-MMP:Fab LEM-2/15, red). No significant spectral changes were detected.

(C and D) Hydrophobic surface presentation of CAT-MT1-MMP. CAT-MT1-MMP is shown as a gray surface, and the hydrophobic side chains are presented in green. (C) shows PDB ID code 3MA2, and (D) shows our TMD structure. The MT1-MMP binding site (V-B loop) to Fab LEM-2/15 is indicated.

(E and F) Surface electrostatic potential of CAT-MT1-MMP. Qualitative calculation of the surface electrostatic potential was done using the PyMOL molecular graphics system (DeLano Scientific). Positive potential is shown in blue, whereas negative potential is shown in red. (E) shows PDB ID code 3MA2, and (F) shows our TMD structure. The MT1-MMP binding site (V-B loop) to Fab LEM-2/15 is indicated.

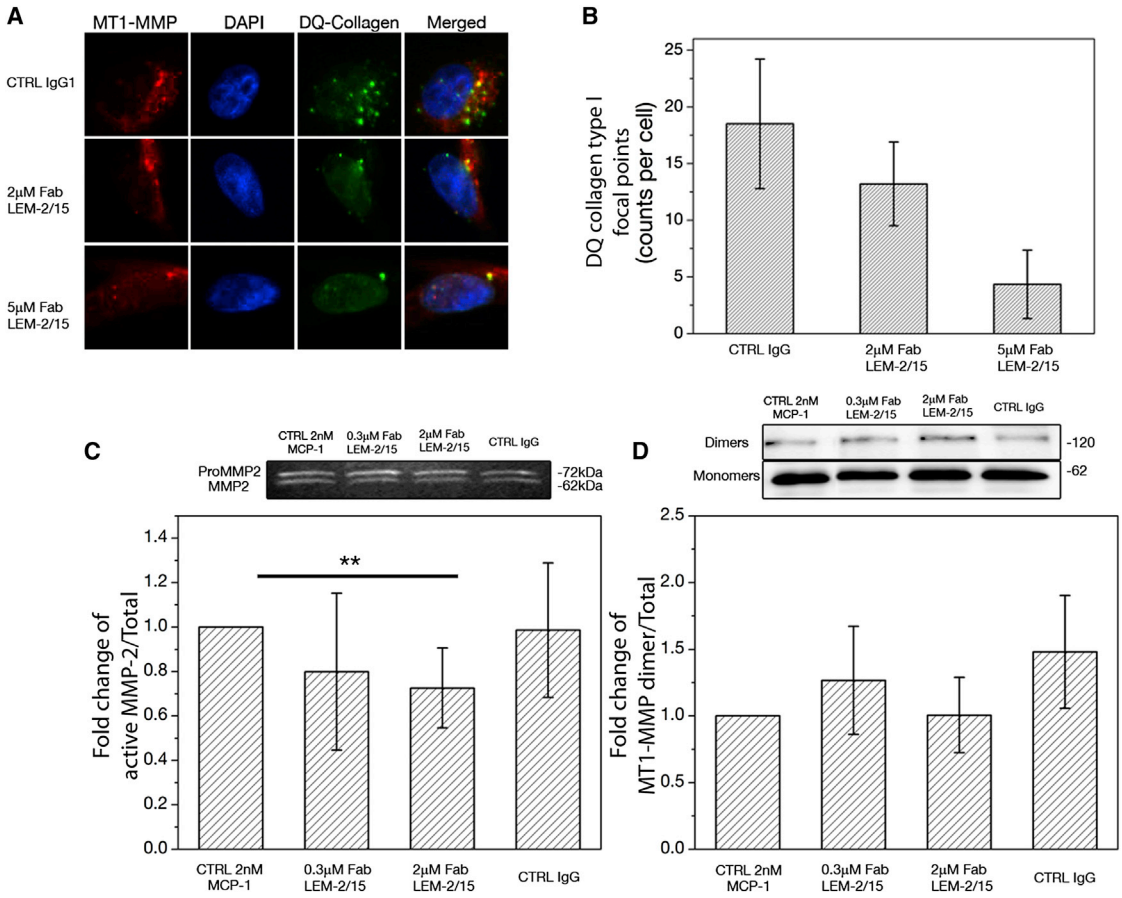

Figure 6. Effect of Fab LEM-2/15 on MT1-MMP Activity in Cells

(A) In situ zymography of collagen type I. HT1080 cells were grown on glass coverslips to adherence. Fab LEM-2/15 was added at 2 and 5 μM and left for 2 hr of incubation at 37°C prior to the addition of DQ-collagen type I. Cells were stained for MT1-MMP and nuclei (DAPI). Clearly, the increase in Fab LEM-2/15 concentration leads to a decrease in DQ-collagen fluorescence because of less degradation by MT1-MMP. CTRL, control.

(B) DQ collagen type I focal points per cell. The data from (A) were quantified, averaged, and plotted as focal points per cell, showing the reduction in collagenolytic activity of MT1-MMP with the increase in concentration of Fab LEM-2/15. Error bars represent SD of the average number of focal points per field of view.

(C and D) Human endothelial cell monolayers were wounded and incubated with MCP-1 for 6 hr in addition to Fab LEM-2/15 or control IgG.

(C) ProMMP-2 activation was assessed by gelatin zymography of culture supernatants. Representative zymograms (top) and bar plots of MMP-2 fold change activation compared with control cells (bottom) are shown ($n \geq 6$ independent experiments). Error bars represent SD of representative experiments.

(D) Plasma membrane-enriched fractions were extracted with Triton X-114, and MT1-MMP dimers were detected by western blot after a nonreducing SDS-PAGE gel. Representative western blots (top) and bar plots of MT1-MMP fold change dimers compared with control cells (bottom) are shown (n = 4 independent experiments). Error bars represent SD of representative experiments.

as specific states of cancer progression in which MMP-2 serves as an antitarget (Overall and Kleifeld, 2006).

The design of future inhibitors possessing molecular interactions with unique surface epitopes having a functional role shows potential promise in improving drug selectivity. However, the main challenge is the identification of such surface epitopes and the design of appropriate antagonist molecules. Our structural study shows that the V-B loop epitope is an ideal candidate for therapeutic design of MT1-MMP inhibition because of its flexibility and conformability, which can be modulated by the binding of function-blocking molecule such as an antibody. This work demonstrates the importance of identifying surface epitopes in the context of their enzymatic function to develop advanced inhibition strategies with improved selectivity.

EXPERIMENTAL PROCEDURES

MT1-MMP Expression and Purification

CAT-MT1-MMP was overexpressed and purified as described previously (Udi et al., 2013).

Antibody Purification

Hybridoma cells of LEM-2/15 were grown in DCCM (serum-free medium designed for hybridoma cell growth and monoclonal antibody production, purchased from Biological Industries). Cells were precipitated by centrifugation at 193 × *g*, and the supernatant was collected. The supernatant was dialyzed against 20 mM phosphate buffer (pH 8). A 1 ml HiTrap protein A high-performance column was equilibrated with 100 mM phosphate buffer (pH 8), and the supernatant was loaded at 1 ml/min. The antibody was eluted with 100 mM citrate buffer (pH 6) and dialyzed against 50 mM Tris (pH 7.5) and 150 mM NaCl.

Antibody Digestion with Papain

Papain was activated in 0.5 M Tris-HCl (pH 8), 10 mM EDTA, and 5mM dithiothreitol for 15 min at 37°C. Active papain was added to a solution of intact LEM-2/15 at a ratio of 1:1,000, and the digestion process was carried out for 3 h at 37°C. The digestion reaction was terminated with the addition of 20 mM iodoacetamide in the dark at room temperature for 30 min. The Fab fragment was isolated from the Fc by a protein A column, and the Fab fragment was collected from the flowthrough and dialyzed against 50 mM Tris-HCl (pH 7.5) and 150 mM NaCl. The purity of the Fab fragment was estimated by 12% SDS-PAGE gel.

Fab Fragment Cloning, Expression, and Purification

The pGD2a phagemid expression vector containing the sequence of the Fab fragment with a His tag at the C terminus was transformed into BL-21 bacteria and grown on a lysogeny broth (LB)/ampicillin plate. Bacteria were grown in LB medium containing 100 μg/ml ampicillin and 0.5% glucose in a shaker flask at 37°C. Protein expression was induced with 0.5 mM isopropyl β-D-1-thiogalactopyranoside at optical density 600 nm = 0.6, and cell growth was continued for a further 16 hr at 16°C. Cells were harvested at 4,200 × *g* for 15 min, and the pellet was suspended in 75 ml ice-cold Tris-HCl (pH 7.4), 20% sucrose, 0.5 mg/ml lysozyme, 10–20 μl DNase I, and 2.5 mM $MgCl_2$. Next, 75 ml of ice-cold water with $MgSO_4$ was added and left on ice for 10 min. The suspension was centrifuged for 40 min at 9,500 × *g*. The supernatant was dialyzed against 50 mM Tris-HCl and 150 mM NaCl and purified on a nickel-nitrilotriacetic acid column.

MT1-MMP ELISA Binding Assay

A 96-well plate (Nunc) was coated with CAT-MMP at 5 μg/ml. After the plate was coated, it was incubated with the Fab LEM-2/15 for 1 hr at 25°C. The bound Fab fragment was detected using a goat anti-Fab antibody followed by peroxidase-conjugated antibody and bovine anti-goat antibody according to standard procedures. The half-maximal effective concentration was calculated from a four-parametric sigmoidal curve-fitting analysis.

SPR Analysis

The affinity between Fab LEM-2/15 and CAT-MT1-MMP was measured with a BIAcore 3000 instrument (Biacore). CAT-MT1-MMP was immobilized on a CM5 sensor chip as described previously (Udi et al., 2013). Each binding experiment was performed with a constant flow of 20 μl/min at 25°C. Sixty microliters of Fab LEM-2/15 (1–20 nM) were injected over the surface for the association phase. The surface was regenerated by the addition of 1 mM NaOH. To estimate the increase in the response diffraction (response units [R.U.]) resulting from nonspecific effects of the protein on the bulk refractive index, the binding of the Fab fragment as a control with no immobilized protein was also measured. This nonspecific signal was subtracted from the measured signal for the interaction between CAT-MT1-MMP and Fab LEM-2/15 at all analyzed concentrations. The data were fitted using a monophasic model for nonlinear curve fitting, taking into account possible mass transport. Kinetic association (*ka*) and dissociation (*kd*) rate constants were calculated using global spectrum analysis as well as by fitting the individual association and dissociation phases using the BIAevaluation 2.1 software package (Pharmacia).

MMP Enzymatic Assay

Kinetic Assays

The enzymatic activity of the CAT-MT1-MMP in the presence of Fab LEM-2/15 was measured at 37°C by monitoring the hydrolysis of the fluorogenic peptide Mca-Pro-Leu-Gly-Leu-Dpa-Ala-Arg-NH_2 at λ_{ex} = 340 nm and λ_{em} = 390 nm as described previously (Knight et al., 1992). A range of different concentrations of Fab LEM-2/15 (0–5,000 nM) were incubated with 10 nM of CAT-MT1-MMP in 50 mM Tris-HCl buffer (pH 7.5 at 37°C), 100 mM NaCl, 5 mM $CaCl_2$, and 0.05% Brij-35 for 2 hr at 37°C. The enzymatic reaction was initiated by addition of the fluorogenic peptide to a final concentration of 10 μM. Fluorescence was recorded immediately and continuously for 30 min. Initial reaction rates were measured, and the inhibition constant was evaluated by fitting the data to the equation

$$\frac{v_i}{v_0}\% = \frac{1}{1+\frac{[I]}{IC_{50}}} \times 100,$$

where v_i is initial velocity in the presence of the inhibitor, v_0 is the initial velocity in the absence of inhibitor, and *I* is the inhibitor concentration.

To determine the type of inhibition, the initial velocity of CAT-MT1-MMP was measured as a function of substrate concentration (0–30 μM) at several fixed concentrations of the Fab LEM-2/15 (between 0–500 nM). The values of apparent K_M and V_{max} were derived by linearization according to the Lineweaver-Burk equation:

$$\frac{1}{V} = \frac{K_M}{V_{max}} \times \frac{1}{[S]} + \frac{1}{V_{max}}.$$

SDS-PAGE Gel Activity Assay

CAT-MT1-MMP (10 nM) was incubated at 37°C for 1 hr in the presence of 1 μM Fab LEM-2/15 and Marimastat and in their absence. After incubation, 1 mg/ml gelatin (porcine skin, Sigma) or rat tail collagen type I (Sigma) was added and left at 37°C. Samples were taken after 5 and 16 hr. The reaction was quenched with 5 μl 4× sample buffer. Next, the samples were analyzed by 12% SDS-PAGE gel.

Cell-Based Assays

In Situ Collagen Type I Zymography

HT1080 cells were cultured on glass coverslips in 24-well tissue culture plates with 300 μl Dulbecco's modified Eagle's medium. After the cells adhered, Fab LEM-2/15 was added for 2 hr of incubation at 37°C prior to substrate addition. 1 mg/ml DQ collagen type I (Molecular Probes) was diluted to 40 μg/ml with 50 mM Tris (pH 7.5), 100 mM NaCl, 5 mM $CaCl_2$, and 0.2 mM sodium azide. Three hundred microliters of the diluted substrate were added, and the reaction was carried out overnight at 37°C. The next day, cells were washed with PBS and fixed with 4% paraformaldehyde.

For immunostaining, cells were permeabilized with 0.5% saponin in PBS for 10 min and washed twice in PBS, and blocked with 1% BSA in PBS for 1 hr, and then anti-mmp14 rabbit (Abcam, catalog no. ab 51074, 1:100 dilution) was added to the blocking solution for 1 hr. Cells were washed twice in PBS, and a secondary antibody, donkey anti-rabbit (Jackson ImmunoResearch Laboratories, catalog no. 711-605-152, 1:200 dilution) was added to the blocking solution for 1 hr. Cells were washed with PBS, and DAPI was added at 2 μg/ml for 10 min. Cells were washed in PBS, dried, mounted with Elvanol, and dried overnight at room temperature. Samples were imaged using a Nikon 80i Eclipse microscope.

Zymography and Western Blot in Human Endothelial Cells

Human umbilical vein endothelial cells (Lonza) were grown to confluence on gelatin and starved in serum-free medium (HE-SFM, Gibco) for 20 hr. Endothelial cell monolayers were then scraped with a "tip" and incubated with 2 nM MCP-1 in the same medium for 6 hr in the presence or absence of Fab LEM-2/15 or complete antibody. Supernatants were collected and analyzed by gelatin zymography (Gálvez et al., 2001a). To test MT1-MMP dimer formation, endothelial cell membranes were extracted in the hydrophobic fraction of 1.5% Triton X-114 lysates and resolved on 10% SDS-PAGE gel under strict nonreducing conditions (Gunasekaran et al., 2004). Quantification was done with ImageJ software.

Protein Crystallography

See Supplemental Experimental Procedures for a detailed description of crystallization conditions, structure determination, and refinement.

ANS Fluorescence Assay

ANS was dissolved in water and filtered. ANS was added (250 μM) to 5 μM CAT-MT1-MMP, Fab LEM, and the complex CAT-MT1-MMP:Fab LEM-2/15. ANS was excited at 350 nm, and the emission spectra were recorded at 400–600nm.

XAS Measurement and Analyses

CAT-MT1-MMP (200 μM final concentration) was incubated at 37°C for 2 hr with Fab LEM-2/15 at 1:1 molar ratios. The sample was loaded, measured, and analyzed as described previously (Solomon et al., 2007; Udi et al., 2013).

MD Simulations and TMD

See Supplemental Experimental Procedures for detailed descriptions of MD simulations and TMD calculations.

ACCESSION NUMBERS

The coordinates and structure factors for the Fab LEM-2/15:MT1-MMP V-B loop (residues 215–227) complex were deposited in the RCSB Protein Data Bank with access codes 4P3D and 4P3C. The coordinates and structure factors for the Fab LEM-2/15:MT1-MMP V-B loop (residues 218–228) complex were deposited in the RCSB Protein Data Bank with access code 4QXU. The coordinates and structure factors for the free form of Fab LEM-2/15 were deposited in the RCSB Protein Data Bank with access code 4OUU.

SUPPLEMENTAL INFORMATION

Supplemental Information includes Supplemental Experimental Procedures, six figures, and three tables and can be found with this article online at http://dx.doi.org/10.1016/j.str.2014.10.012.

AUTHOR CONTRIBUTIONS

Y.U. designed the experiments, conducted the research, analyzed the data, and wrote the manuscript. M.G. and I. Solomonov assisted with protein purification and data analysis and wrote the manuscript. A.A. and I. Sagi designed the experiments and wrote the manuscript. O.D. and H.R. collected crystallographic data and determined the structures. V.M. conducted the dimerization and activation experiments. P.C. and V.D. performed the TMD simulations.

ACKNOWLEDGMENTS

We would like to thank Elad Bassat from the Department of Biological Regulation at the Weizmann Institute and Ángela Pollán from the Department of Vascular Biology and Inflammation, Centro Nacional de Investigaciones Cardiovasculares (CNIC) for help and technical support. The research leading to these results has received funding from the Israeli Scientific Foundation, EU FP7, and SaveMe project. I.S. is the incumbent of the Pontecorvo professorial chair. V.M. is supported by the Regional Government of 654 Madrid, Spain (Angiobodies Programme, S2010/BMD-2312).

Received: May 22, 2014
Revised: October 7, 2014
Accepted: October 13, 2014
Published: December 4, 2014

REFERENCES

Arighi, C.N., Rossi, J.P., and Delfino, J.M. (1998). Temperature-induced conformational transition of intestinal fatty acid binding protein enhancing ligand binding: a functional, spectroscopic, and molecular modeling study. Biochemistry *37*, 16802–16814.

Bahar, I., Chennubhotla, C., and Tobi, D. (2007). Intrinsic dynamics of enzymes in the unbound state and relation to allosteric regulation. Curr. Opin. Struct. Biol. *17*, 633–640.

Bhaskaran, R., Palmier, M.O., Lauer-Fields, J.L., Fields, G.B., and Van Doren, S.R. (2008). MMP-12 catalytic domain recognizes triple helical peptide models of collagen V with exosites and high activity. J. Biol. Chem. *283*, 21779–21788.

Bode, W., Gomis-Rüth, F.X., and Stöckler, W. (1993). Astacins, serralysins, snake venom and matrix metalloproteinases exhibit identical zinc-binding environments (HEXXHXXGXXH and Met-turn) and topologies and should be grouped into a common family, the 'metzincins'. FEBS Lett. *331*, 134–140.

Brinckerhoff, C.E., and Matrisian, L.M. (2002). Matrix metalloproteinases: a tail of a frog that became a prince. Nat. Rev. Mol. Cell Biol. *3*, 207–214.

Browner, M.F., Smith, W.W., and Castelhano, A.L. (1995). Matrilysin-inhibitor complexes: common themes among metalloproteases. Biochemistry *34*, 6602–6610.

Butler, G.S., Butler, M.J., Atkinson, S.J., Will, H., Tamura, T., Schade van Westrum, S., Crabbe, T., Clements, J., d'Ortho, M.P., and Murphy, G. (1998). The TIMP2 membrane type 1 metalloproteinase "receptor" regulates the concentration and efficient activation of progelatinase A. A kinetic study. J. Biol. Chem. *273*, 871–880.

Choi, K.Y., Swierczewska, M., Lee, S., and Chen, X. (2012). Protease-activated drug development. Theranostics *2*, 156–178.

Chothia, C., Lesk, A.M., Tramontano, A., Levitt, M., Smith-Gill, S.J., Air, G., Sheriff, S., Padlan, E.A., Davies, D., Tulip, W.R., et al. (1989). Conformations of immunoglobulin hypervariable regions. Nature *342*, 877–883.

Chung, L., Shimokawa, K., Dinakarpandian, D., Grams, F., Fields, G.B., and Nagase, H. (2000). Identification of the (183)RWTNNFREY(191) region as a critical segment of matrix metalloproteinase 1 for the expression of collagenolytic activity. J. Biol. Chem. *275*, 29610–29617.

Coussens, L.M., Fingleton, B., and Matrisian, L.M. (2002). Matrix metalloproteinase inhibitors and cancer: trials and tribulations. Science *295*, 2387–2392.

Cuniasse, P., Devel, L., Makaritis, A., Beau, F., Georgiadis, D., Matziari, M., Yiotakis, A., and Dive, V. (2005). Future challenges facing the development of specific active-site-directed synthetic inhibitors of MMPs. Biochimie *87*, 393–402.

DeClerck, Y.A., and Imren, S. (1994). Protease inhibitors: role and potential therapeutic use in human cancer. Eur. J. Cancer *30A*, 2170–2180.

Deu, E., Verdoes, M., and Bogyo, M. (2012). New approaches for dissecting protease functions to improve probe development and drug discovery. Nat. Struct. Mol. Biol. *19*, 9–16.

Fernandez-Catalan, C., Bode, W., Huber, R., Turk, D., Calvete, J.J., Lichte, A., Tschesche, H., and Maskos, K. (1998). Crystal structure of the complex formed by the membrane type 1-matrix metalloproteinase with the tissue inhibitor of metalloproteinases-2, the soluble progelatinase A receptor. EMBO J. *17*, 5238–5248.

Fisher, J.F., and Mobashery, S. (2006). Recent advances in MMP inhibitor design. Cancer Metastasis Rev. *25*, 115–136.

Frenkel, A.I., Kleifeld, O., Wasserman, S.R., and Sagi, I. (2002). Phase speciation by extended x-ray absorption fine structure spectroscopy. J. Chem. Phys. *116*, 9449–9456.

Gálvez, B.G., Matías-Román, S., Albar, J.P., Sánchez-Madrid, F., and Arroyo, A.G. (2001a). Membrane type 1-matrix metalloproteinase is activated during migration of human endothelial cells and modulates endothelial motility and matrix remodeling. J. Biol. Chem. *276*, 37491–37500.

Genís, L., Gálvez, B.G., Gonzalo, P., and Arroyo, A.G. (2006). MT1-MMP: universal or particular player in angiogenesis? Cancer Metastasis Rev. *25*, 77–86.

Grossman, M., Tworowski, D., Dym, O., Lee, M.H., Levy, Y., Murphy, G., and Sagi, I. (2010). The intrinsic protein flexibility of endogenous protease inhibitor TIMP-1 controls its binding interface and affects its function. Biochemistry *49*, 6184–6192.

Grossman, M., Born, B., Heyden, M., Tworowski, D., Fields, G.B., Sagi, I., and Havenith, M. (2011). Correlated structural kinetics and retarded solvent dynamics at the metalloprotease active site. Nat. Struct. Mol. Biol. *18*, 1102–1108.

Gunasekaran, K., Ma, B., and Nussinov, R. (2004). Is allostery an intrinsic property of all dynamic proteins? Proteins *57*, 433–443.

Itoh, Y., Ito, N., Nagase, H., Evans, R.D., Bird, S.A., and Seiki, M. (2006). Cell surface collagenolysis requires homodimerization of the membrane-bound collagenase MT1-MMP. Mol. Biol. Cell *17*, 5390–5399.

Jiang, A., Lehti, K., Wang, X., Weiss, S.J., Keski-Oja, J., and Pei, D. (2001). Regulation of membrane-type matrix metalloproteinase 1 activity by dynamin-mediated endocytosis. Proc. Natl. Acad. Sci. USA *98*, 13693–13698.

Kawasaki, G., Kato, Y., and Mizuno, A. (2002). Cathepsin expression in oral squamous cell carcinoma: relationship with clinicopathologic factors. Oral Surg. Oral Med. Oral Pathol. Oral Radiol. Endod. *93*, 446–454.

Kay, L.E., Nicholson, L.K., Delaglio, F., Bax, A., and Torchia, D.A. (1992). Pulse sequences for removal of the effects of cross correlation between dipolar and chemical-shift anisotropy relaxation mechanism on the measurement of heteronuclear T_1 and T_2 values in proteins. J. Magn. Reson. *97*, 359–375.

Knäuper, V., Will, H., López-Otin, C., Smith, B., Atkinson, S.J., Stanton, H., Hembry, R.M., and Murphy, G. (1996). Cellular mechanisms for human procollagenase-3 (MMP-13) activation. Evidence that MT1-MMP (MMP-14) and

gelatinase a (MMP-2) are able to generate active enzyme. J. Biol. Chem. *271*, 17124–17131.

Knight, C.G., Willenbrock, F., and Murphy, G. (1992). A novel coumarin-labelled peptide for sensitive continuous assays of the matrix metalloproteinases. FEBS Lett. *296*, 263–266.

Koblinski, J.E., Ahram, M., and Sloane, B.F. (2000). Unraveling the role of proteases in cancer. Clin. Chim. Acta *291*, 113–135.

Koshland, D.E., Jr., and Hamadani, K. (2002). Proteomics and models for enzyme cooperativity. J. Biol. Chem. *277*, 46841–46844.

Koziol, A., Gonzalo, P., Mota, A., Pollán, Á., Lorenzo, C., Colomé, N., Montaner, D., Dopazo, J., Arribas, J., Canals, F., and Arroyo, A.G. (2012a). The protease MT1-MMP drives a combinatorial proteolytic program in activated endothelial cells. FASEB J. *26*, 4481–4494.

Koziol, A., Martín-Alonso, M., Clemente, C., Gonzalo, P., and Arroyo, A.G. (2012b). Site-specific cellular functions of MT1-MMP. Eur. J. Cell Biol. *91*, 889–895.

Lehti, K., Valtanen, H., Wickström, S.A., Lohi, J., and Keski-Oja, J. (2000). Regulation of membrane-type-1 matrix metalloproteinase activity by its cytoplasmic domain. J. Biol. Chem. *275*, 15006–15013.

Liu, Z., Zhou, X., Shapiro, S.D., Shipley, J.M., Twining, S.S., Diaz, L.A., Senior, R.M., and Werb, Z. (2000). The serpin alpha1-proteinase inhibitor is a critical substrate for gelatinase B/MMP-9 in vivo. Cell *102*, 647–655.

López-Otín, C., and Matrisian, L.M. (2007a). Emerging roles of proteases in tumour suppression. Nat. Rev. Cancer *7*, 800–808.

López-Otín, C., and Overall, C.M. (2002). Protease degradomics: a new challenge for proteomics. Nat. Rev. Mol. Cell Biol. *3*, 509–519.

McQuibban, G.A., Gong, J.H., Tam, E.M., McCulloch, C.A., Clark-Lewis, I., and Overall, C.M. (2000). Inflammation dampened by gelatinase A cleavage of monocyte chemoattractant protein-3. Science *289*, 1202–1206.

Mergulhão, F.J.M., Summers, D.K., and Monteiro, G.A. (2005). Recombinant protein secretion in Escherichia coli. Biotechnol. Adv. *23*, 177–202.

Monod, J., Wyman, J., and Changeux, J.P. (1965). On the Nature of Allosteric Transitions: A Plausible Model. J. Mol. Biol. *12*, 88–118.

Morrison, C.J., Butler, G.S., Rodríguez, D., and Overall, C.M. (2009). Matrix metalloproteinase proteomics: substrates, targets, and therapy. Curr. Opin. Cell Biol. *21*, 645–653.

Nagase, H., and Woessner, J.F., Jr. (1999). Matrix metalloproteinases. J. Biol. Chem. *274*, 21491–21494.

Nakahara, H., Howard, L., Thompson, E.W., Sato, H., Seiki, M., Yeh, Y., and Chen, W.T. (1997). Transmembrane/cytoplasmic domain-mediated membrane type 1-matrix metalloprotease docking to invadopodia is required for cell invasion. Proc. Natl. Acad. Sci. USA *94*, 7959–7964.

Overall, C.M. (2002). Molecular determinants of metalloproteinase substrate specificity: matrix metalloproteinase substrate binding domains, modules, and exosites. Mol. Biotechnol. *22*, 51–86.

Overall, C.M., and Kleifeld, O. (2006). Tumour microenvironment - opinion: validating matrix metalloproteinases as drug targets and anti-targets for cancer therapy. Nat. Rev. Cancer *6*, 227–239.

Overall, C.M., and López-Otín, C. (2002). Strategies for MMP inhibition in cancer: innovations for the post-trial era. Nat. Rev. Cancer *2*, 657–672.

Palmier, M.O., Fulcher, Y.G., Bhaskaran, R., Duong, V.Q., Fields, G.B., and Van Doren, S.R. (2010). NMR and bioinformatics discovery of exosites that tune metalloelastase specificity for solubilized elastin and collagen triple helices. J. Biol. Chem. *285*, 30918–30930.

Pelman, G.R., Morrison, C.J., and Overall, C.M. (2005). Pivotal molecular determinants of peptidic and collagen triple helicase activities reside in the S3′ subsite of matrix metalloproteinase 8 (MMP-8): the role of hydrogen bonding potential of ASN188 and TYR189 and the connecting cis bond. J. Biol. Chem. *280*, 2370–2377.

Raha, T., Chattopadhyay, D., Chattopadhyay, D., and Roy, S. (1999). A phosphorylation-induced major structural change in the N-terminal domain of the P protein of Chandipura virus. Biochemistry *38*, 2110–2116.

Rao, B.G. (2005). Recent developments in the design of specific Matrix Metalloproteinase inhibitors aided by structural and computational studies. Curr. Pharm. Des. *11*, 295–322.

Rasmussen, H.S., and McCann, P.P. (1997). Matrix metalloproteinase inhibition as a novel anticancer strategy: a review with special focus on batimastat and marimastat. Pharmacol. Ther. *75*, 69–75.

Roghi, C., Jones, L., Gratian, M., English, W.R., and Murphy, G. (2010). Golgi reassembly stacking protein 55 interacts with membrane-type (MT) 1-matrix metalloprotease (MMP) and furin and plays a role in the activation of the MT1-MMP zymogen. FEBS J. *277*, 3158–3175.

Rozanov, D.V., Ghebrehiwet, B., Ratnikov, B., Monosov, E.Z., Deryugina, E.I., and Strongin, A.Y. (2002). The cytoplasmic tail peptide sequence of membrane type-1 matrix metalloproteinase (MT1-MMP) directly binds to gC1qR, a compartment-specific chaperone-like regulatory protein. FEBS Lett. *527*, 51–57.

Sato, H., Takino, T., Okada, Y., Cao, J., Shinagawa, A., Yamamoto, E., and Seiki, M. (1994). A matrix metalloproteinase expressed on the surface of invasive tumour cells. Nature *370*, 61–65.

Seiki, M. (2003). Membrane-type 1 matrix metalloproteinase: a key enzyme for tumor invasion. Cancer Lett. *194*, 1–11.

Sela-Passwell, N., Rosenblum, G., Shoham, T., and Sagi, I. (2010). Structural and functional bases for allosteric control of MMP activities: can it pave the path for selective inhibition? Biochim. Biophys. Acta *1803*, 29–38.

Sharma, S.K., ed. (2012). X-Ray Spectroscopy (Rijeka: INTECH).

Solomon, A., Akabayov, B., Frenkel, A., Milla, M.E., and Sagi, I. (2007). Key feature of the catalytic cycle of TNF-alpha converting enzyme involves communication between distal protein sites and the enzyme catalytic core. Proc. Natl. Acad. Sci. USA *104*, 4931–4936.

Strongin, A.Y., Collier, I., Bannikov, G., Marmer, B.L., Grant, G.A., and Goldberg, G.I. (1995). Mechanism of cell surface activation of 72-kDa type IV collagenase. Isolation of the activated form of the membrane metalloprotease. J. Biol. Chem. *270*, 5331–5338.

Taniwaki, K., Fukamachi, H., Komori, K., Ohtake, Y., Nonaka, T., Sakamoto, T., Shiomi, T., Okada, Y., Itoh, T., Itohara, S., et al. (2007). Stroma-derived matrix metalloproteinase (MMP)-2 promotes membrane type 1-MMP-dependent tumor growth in mice. Cancer Res. *67*, 4311–4319.

Turk, B. (2006a). Targeting proteases: successes, failures and future prospects. Nat. Rev. Drug Discov. *5*, 785–799.

Udi, Y., Fragai, M., Grossman, M., Mitternacht, S., Arad-Yellin, R., Calderone, V., Melikian, M., Toccafondi, M., Berezovsky, I.N., Luchinat, C., and Sagi, I. (2013). Unraveling hidden regulatory sites in structurally homologous metalloproteases. J. Mol. Biol. *425*, 2330–2346.

Uekita, T., Itoh, Y., Yana, I., Ohno, H., and Seiki, M. (2001). Cytoplasmic tail-dependent internalization of membrane-type 1 matrix metalloproteinase is important for its invasion-promoting activity. J. Cell Biol. *155*, 1345–1356.

Wang, X., Ma, D., Keski-Oja, J., and Pei, D. (2004). Co-recycling of MT1-MMP and MT3-MMP through the trans-Golgi network. Identification of DKV582 as a recycling signal. J. Biol. Chem. *279*, 9331–9336.

Wilson, I.A., and Stanfield, R.L. (1994). Antibody-antigen interactions: new structures and new conformational changes. Curr. Opin. Struct. Biol. *4*, 857–867.

Wilson, C.L., Ouellette, A.J., Satchell, D.P., Ayabe, T., López-Boado, Y.S., Stratman, J.L., Hultgren, S.J., Matrisian, L.M., and Parks, W.C. (1999). Regulation of intestinal alpha-defensin activation by the metalloproteinase matrilysin in innate host defense. Science *286*, 113–117.